



UNIVERSITY OF LEEDS

This is a repository copy of *Evaluation of Novel Routes for NO_x Formation in Remote Regions*.

White Rose Research Online URL for this paper:
<http://eprints.whiterose.ac.uk/118767/>

Version: Accepted Version

Article:

Ye, C, Heard, DE orcid.org/0000-0002-0357-6238 and Whalley, LK
orcid.org/0000-0002-4486-9029 (2017) Evaluation of Novel Routes for NO_x Formation in Remote Regions. *Environmental Science and Technology*, 51 (13). pp. 7442-7449. ISSN 0013-936X

<https://doi.org/10.1021/acs.est.6b06441>

(c) 2017, American Chemical Society. This document is the Accepted Manuscript version of a Published Work that appeared in final form in *Environmental Science and Technology*, copyright (c) American Chemical Society after peer review and technical editing by the publisher. To access the final edited and published work see [<https://doi.org/10.1021/acs.est.6b06441>]

Reuse

See Attached

Takedown

If you consider content in White Rose Research Online to be in breach of UK law, please notify us by emailing eprints@whiterose.ac.uk including the URL of the record and the reason for the withdrawal request.



eprints@whiterose.ac.uk
<https://eprints.whiterose.ac.uk/>

Evaluation of novel routes for NO_x formation in remote regions

Chunxiang Ye, Dwayne E. Heard, and Lisa K. Whalley

Environ. Sci. Technol., **Just Accepted Manuscript** • DOI: 10.1021/acs.est.6b06441 • Publication Date (Web): 05 Jun 2017

Downloaded from <http://pubs.acs.org> on June 15, 2017

Just Accepted

“Just Accepted” manuscripts have been peer-reviewed and accepted for publication. They are posted online prior to technical editing, formatting for publication and author proofing. The American Chemical Society provides “Just Accepted” as a free service to the research community to expedite the dissemination of scientific material as soon as possible after acceptance. “Just Accepted” manuscripts appear in full in PDF format accompanied by an HTML abstract. “Just Accepted” manuscripts have been fully peer reviewed, but should not be considered the official version of record. They are accessible to all readers and citable by the Digital Object Identifier (DOI®). “Just Accepted” is an optional service offered to authors. Therefore, the “Just Accepted” Web site may not include all articles that will be published in the journal. After a manuscript is technically edited and formatted, it will be removed from the “Just Accepted” Web site and published as an ASAP article. Note that technical editing may introduce minor changes to the manuscript text and/or graphics which could affect content, and all legal disclaimers and ethical guidelines that apply to the journal pertain. ACS cannot be held responsible for errors or consequences arising from the use of information contained in these “Just Accepted” manuscripts.

Evaluation of novel routes for NO_x formation in remote regions

Chunxiang Ye^{1,*}, Dwayne E. Heard^{1,2,*} and Lisa K. Whalley^{1,2,*}

¹School of Chemistry, University of Leeds, Leeds, LS2 9JT, UK

²National Centre for Atmospheric Science, University of Leeds, Leeds, LS2 9JT, UK.

Contact information for corresponding author:

School of Chemistry,

University of Leeds,

Leeds,

LS2 9JT, UK.

Tel: 0113 343 6471

Fax: 0113 343 6401

Email: C.Ye@leeds.ac.uk, L.K.Whalley@leeds.ac.uk, D.E.Heard@leeds.ac.uk

Supporting Information.

Figure showing diel profiles of the photolysis rate constants of gas-phase HNO₃ and surface HNO₃; Figure showing The variability of normalized $j_{pNitrate \rightarrow HONO}^N$ and the ratio of $j_{pNitrate \rightarrow HONO}$ to $j_{surface\ nitrate}$ (the scaling factor \emptyset in Eq. 4) on different days during the 2007 RHaMBLe project. Table showing comparison of the conditions for two background marine boundary layer, namely Cape Verde in the RHaMBLe study (used in this study) and the North Atlantic Ocean in the NOMADSS study.

INTRODUCTION

Tropospheric ozone (O_3) is a major atmospheric oxidant and greenhouse gas, and an important precursor of hydroxyl radical (OH), which determines the atmospheric lifetime of “primary” gaseous pollutants, such as methane (CH_4), volatile organic carbon species (VOCs) and carbon monoxide (CO). During the catalytic oxidation of these primary gas pollutants in the presence of NO_x ($=NO + NO_2$), O_3 is produced. Currently, global models can only capture half of the historical and present-day trends of O_3 concentration change and there is a general overestimation (which varies with season and continent) of background O_3 abundance.¹⁻³ The discrepancy between O_3 modelled and measured may partly be attributed to the uncertainties in the assessment of transport and emission terms in global models.¹⁻³ Additionally, however, this discrepancy could suggest that our current understanding in O_3 chemistry is not yet complete.

Photolysis of NO_2 is the only chemical source of O_3 in the troposphere. O_3 production is known not to be linearly correlated with NO_x abundance, but is mediated by NO_x , with the highest ozone production efficiency in low- NO_x regimes.^{4,5} As such, a small change in NO_x abundance in remote regions would result in significant perturbation to O_3 chemistry.^{4,5} However, global networks for routine NO_x measurements in remote regions are not available and long-term NO_x measurements in low- NO_x regime are rare. NO_x observations have been made at the Cape Verde Atmospheric Observatory (CVAO) since 2006 and short-term ship and aircraft measurements in intensive field campaigns have been reported from limited locations.^{4,6,7} Column NO_x is not an ideal input parameter in O_3 models owing to its poor spatial resolution.⁸ Models in the pristine marine boundary layer (MBL), terrestrial areas and free troposphere over-predict nitric acid (HNO_3) or particulate nitrate levels, and under-predict NO_x abundance and NO_x/HNO_3 ratios.^{1,4,5,7-11} For instance, a reduction to 75% of the predicted HNO_3 level was needed to reproduce observations of tropospheric particulate nitrate in a GEOS-Chem study over the United States.¹⁰ These discrepancies between models and observations indicate that either a slower NO_x oxidation rate than is recommended is required or a renoxification process which recycles NO_x from its

oxidation products is missing from global model mechanisms. Lowering the rate constant for reaction of NO_2 with OH within its uncertainty does improve the agreement between models and observations, but cannot fully account for the discrepancy.^{4,5} Most global models and even the near-explicit box model mechanisms often fail to include all important NO_x oxidation routes, such as reactions between NO and RO_2 radicals in forested areas¹²⁻¹⁴ and reactions of NO_2 with halogen oxides (mainly BrO and IO) in the MBL.^{1,4,5,7-11,15,16} Incorporation of these additional NO_x oxidation routes, however, actually worsens the agreement between NO_x observations and models.¹⁵ The lack of a noontime minimum in the NO_2 observations in the remote MBL which has little NO_x emissions suggests an unknown NO_x source to compensate the fast NO_2 photolysis and oxidation losses.^{4,17} Several reactive nitrogen reservoirs, such as PAN and organic nitrates, would help to sustain a critical level of NO_x in the background areas.^{6,13,14} However, the low concentration of PAN means that it is not sufficient to fully account for the discrepancy in the warm MBL,^{4,6,16} and the role of organic nitrates in environments other than the background terrestrial boundary layer has not been explored.¹²⁻¹⁴ In fact, PAN and organic nitrates are observed to have a noontime-to-afternoon maxima together with their precursors, such as the peroxyacetyl radical and peroxy radicals (RO_2), suggesting that they act as NO_x sinks, rather than NO_x sources at this time.^{6,13,18} Photolysis of nitrate associated with urban grime is largely enhanced in the laboratory.^{19,20} Photolysis of particulate nitrate, associated with aged sea spray aerosol, has been observed to proceed at a rate that is at least two orders of magnitude faster than photolysis of gaseous HNO_3 in clean MBL over the Atlantic Ocean, based on laboratory, model and observational evidences.¹⁵ Gas-phase nitrous acid (HONO) and NO_2 were identified as the main products, suggesting that this NO_x recycling route may be essential to reconcile the daytime NO_x discrepancy between models and observations in low- NO_x regimes.

The inclusion of this novel NO_x recycling route is still not fully tested against measured diel profiles of NO_x and the impact of this novel NO_x source on O_3 chemistry in the MBL has not been discussed. Here we present a 0-D box model study employing the near-explicit Master Chemistry Mechanism (MCM v3.2) and comprehensive published measurements of species involved in NO_x and O_3 chemistry at CVAO. Our results

show this novel NO_x recycling route is critical to reproduce NO_x observations during the daytime, and helps to better constrain O₃ formation in the marine boundary layer.

EXPERIMENTAL SECTION

Measurements The Reactive Halogens in the Marine Boundary Layer (RHAMBLE) project was an intensive measurement campaign at CVAO from May 18th – June 15th 2007. Comprehensive measurements including OH and hydroperoxy radicals (HO₂), BrO, IO, O₃, HONO, NO_x, HNO₃, particulate nitrate, total reactive nitrogen (NO_y), aerosol density, aerosol chemical composition, C1 - C5 hydrocarbons, and photolysis frequency of O₃ (J(O¹D)), together with meteorological parameters were available.^{4, 21-28} Other clear sky photolysis frequencies were calculated by the model and scaled by the ratio of observed J(O¹D) : clear sky J(O¹D) to account for cloud cover.²⁹ The measurement techniques are summarized in references.^{21, 22} Briefly, NO, NO₂ and total reactive nitrogen (NO_y) were measured by a chemiluminescence method (with photolytic and catalytic conversion to NO for NO₂ and NO_y respectively).^{4, 21} HNO₃ and HONO were measured by a mist chamber coupled with ion chromatography (IC).²⁵ Aerosol chemical composition, including particulate nitrate concentration, was measured by a filter method coupled with IC.³⁰ Radicals (OH and HO₂) were measured by laser induced fluorescence spectroscopy and the halogen oxides, IO and BrO, were measured by a long-path DOAS system.^{23, 31} The model was constrained to the measurements of VOCs and other long-lived species made during the RHAMBLE project.²² The model calculation was compared with the average diel profiles of HONO and NO_x measured during the RHAMBLE project.

Model description A box model containing the chemical scheme for the oxidation of C1 - C5 alkanes and alkenes, extracted from the Master Chemical Mechanism version 3.2¹⁶ was employed. Additional inorganic chemical reactions were included, both in the gas phase and the aerosol phase. Specifically, a halogen chemical scheme was added to reflect its perturbation to NO_x and HO_x chemistry (such as R1 and R1').^{23, 32} Surface reactions and deposition processes were included, as outlined in references.^{23, 32} The uptake and hydrolysis of the

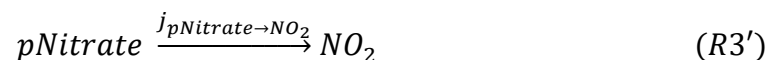
oxidation products of NO_x , e.g., halogen nitrate (XNO_3 ; $\text{X} = \text{Br}$ and I) and organic nitrate (RONO_2) from reactions of NO_2 with XO and of NO with RO_2 on aerosols were included, to reflect their roles as NO_x sinks in the MBL (R1 and R2).^{14, 15, 18, 33} The uptake coefficient of 0.8 for XNO_3 onto aerosols was updated according to the latest JPL recommendation.³⁴ The aerosol uptake coefficient of 10^{-3} for RONO_2 was assumed leading to a hydrolysis lifetime of around 3 hours for RONO_2 in the MBL.^{12, 14}



$\text{HNO}_3(s)$ represents particulate nitrate which is formed within aerosol particles or is in equilibrium with HNO_3 in the gas phase. The concentration of unmeasured intermediate species, generated during the oxidative degradation of inorganic and organic compounds, were initialized at zero and given a first order deposition loss term (~ 24 hr lifetime) to prevent build up to unrealistic levels.²³ The model results presented are relatively insensitive to the deposition rate chosen, however. A steady state concentration of PAN of several tens of p.p.t.v. was calculated by the model but was high compared to the observation of PAN at the low p.p.t.v. level.^{4, 6} Decreasing the formation rate of PAN by a factor of ten reduced the modelled concentration in line with the PAN observations.^{4, 6}

A particulate nitrate-HONO- NO_x photochemical cycling mechanism (R3 and R3') was incorporated into the model mechanism. The total production rate of HONO and NO_2 from particulate nitrate photolysis were determined from the concentration ($[p\text{Nitrate}]$) and photolysis rate constant of particulate nitrate ($j_{p\text{Nitrate}}$, Eq. 1), ($[p\text{Nitrate}] \times j_{p\text{Nitrate}}$).¹⁵

$$j_{p\text{Nitrate}} = j_{p\text{Nitrate} \rightarrow \text{HONO}} + j_{p\text{Nitrate} \rightarrow \text{NO}_2} \quad (\text{Eq. 1})$$



where $j_{p\text{Nitrate} \rightarrow \text{HONO}}$ and $j_{p\text{Nitrate} \rightarrow \text{NO}_2}$ are the formation rate constants of HONO and NO_2 from particulate nitrate photolysis, respectively. The dominant HONO sink was photolysis, and the major sinks of NO_x were oxidation routes, such as R1, R2 and R5. These HONO and NO_x sinks are well constrained with measured parameters in the box model for this low- NO_x MBL environment (see HONO and NO_x budget analysis in discussion section). Therefore, HONO and NO_2 production rates from particulate nitrate photolysis could be reasonably well constrained by balancing the HONO and NO_x budgets. For example, a simplified HONO and NO_x budget may be summarized as (Eq. 2 and 2'):

$$[p\text{Nitrate}] \times j_{p\text{Nitrate} \rightarrow \text{HONO}} \approx [\text{HONO}] \times j_{\text{HONO}} \quad (\text{Eq. 2})$$

$$[p\text{Nitrate}] \times (j_{p\text{Nitrate} \rightarrow \text{HONO}} + j_{p\text{Nitrate} \rightarrow \text{NO}_2}) \approx L(\text{NO}_x) \quad (\text{Eq. 2}')$$

where $[\text{HONO}]$ represents the observed mixing ratios of HONO, j_{HONO} represents the photolysis rate constant of HONO,²⁹ and $L(\text{NO}_x)$ represents the sum of oxidation rates of NO_x to HNO_3 , halogen nitrate and organic nitrate (see “ NO_x budget analysis” section). As $[p\text{Nitrate}]$, $[\text{HONO}]$ and j_{HONO} are known, it becomes possible to estimate $j_{p\text{Nitrate} \rightarrow \text{HONO}}$ in Eq. 2. The error in the calculation of $j_{p\text{Nitrate} \rightarrow \text{HONO}}$ via Eq.2 is 35%, taking into account the uncertainties ($\pm 20\%$) in the measurements of j_{HONO} , HONO and particulate nitrate.

For comparison, the diel profile of the photolysis rate constant for nitrate absorbed on silicon surface ($j_{\text{surface nitrate}}$) can be calculated from the product of the published cross sections, quantum yield, and the campaign relevant actinic flux, integrated between 290 - 365 nm (Eq. 3). This photolysis rate constant is found to be at least three orders of magnitude larger than the photolysis frequency of gaseous HNO_3 , j_{HNO_3} (supplementary information, Figure S1).^{35, 36} If the physical and chemical state of nitrate on a silicon

surface and particulate nitrate is similar (and that this state determines the absorption spectrum and photochemical reactivity), then $j_{surface\ nitrate}$ can be equated to $j_{pNitrate}$.³⁷ In reality, however, it is likely that the physical and chemical state of nitrate on a silicon surface and particulate nitrate in marine aerosols is not the same and so we have used a scaling factor, \emptyset , to represent both the quantum yield of HONO from particulate nitrate photolysis as well as any differences in absorption cross sections which arise as a result of the different surface properties of silicon and particulate nitrate (Eq. 4):

$$j_{surface\ nitrate} = \int_{290\ nm}^{365\ nm} I(\lambda)\sigma(\lambda)\phi(\lambda)d\lambda \quad (Eq. 3)$$

$$j_{pNitrate \rightarrow HONO} = \emptyset \times j_{surface\ nitrate} \quad (Eq. 4)$$

where $I(\lambda)$, $\sigma(\lambda)$, and $\phi(\lambda)$ are the wavelength dependent actinic flux, absorption cross section and quantum yield for surface nitrate, respectively. $I(\lambda)$ was calculated using the tropospheric ultraviolet and visible (TUV) radiation model and was further scaled by the ratio of measured $J(O^1D)$: calculated clear sky $J(O^1D)$ to account for cloud cover.²⁹ $\sigma(\lambda)$ and $\phi(\lambda)$ were taken from the literature.^{35, 36}

Similarly, the scaling factor for $j_{pNitrate \rightarrow NO_2}$ can be determined in a balanced NO_x budget (Eq. 2'), taking into account that HONO produced in particulate nitrate photolysis is an intermediate to NO_x , via photolysis (R4).



No transport processes were considered in the model, only photochemical processes. As such, we focus the comparisons between model and observation on the daytime only. Model runs with and without the particulate nitrate photolysis mechanism are referred to as “Photolytic” model and “Baseline” model respectively.

For NO_x , HNO_3 and O_3 , the model was constrained to the observations just after sunrise (8:15 a.m. local time), but then allowed to vary for the rest of the day.⁴ The model was initialised at midday on the first day and allowed to run for several days with a time-step of half an hour until the concentration of the intermediate species reached steady state. The model results were then compared to measurements of HONO and NO_x . The modelled diurnals of species (e.g. HO_x) were identical after the first two days of simulations, suggesting that steady state conditions were reached from the third day onwards, and hence the results shown here were all from the fourth day following initiation.

Radicals are able to perturb the NO_x budget and NO_2/NO ratio via reactions such as R2, R5, R6 and R6'.

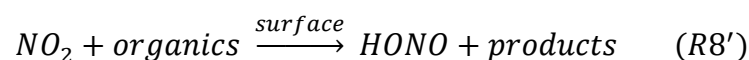


The box model including these reactions was able to reproduce OH and HO_2 radicals at Cape Verde²¹, and RO_2 radicals in the Southern Atlantic ocean,^{23, 38} and so these radical-related NO_x sink terms can be considered to be well constrained in our study.

RESULTS

HONO calculation. Figure 1 shows the diel profiles of observed and modelled HONO concentrations and observed $\text{J}(\text{O}^1\text{D})$. To evaluate the photolysis mechanism and its impact on daytime NO_x abundance, the model and observations were compared between 10:00 and 16:00 (local time), approximately two hours after sunrise and two hours before sunset. HONO observations showed a daytime peak occurring slightly earlier than solar noon, and a nighttime minima of around 1 p.p.t.v..³⁹ The mean ($\pm 1\sigma$) of the HONO daytime peak is 5.2 (± 4.0) p.p.t.v. and ranged from 3 to 16 p.p.t.v.. This diurnal profile suggests a photochemical source of HONO in the

MBL.¹⁵ By comparison, a noontime HONO mixing ratio of 8 - 12 p.p.t.v. was reported for two days in the Atlantic Ocean off the Southeast US coast in the NOMADSS study and the photochemical source of HONO was proposed to be particulate nitrate photolysis (referred to here as the “NOMADSS scenario”).¹⁵ A comparison of the different chemical environments for the RHaMBLe project and the “NOMADSS scenario” is summarized in the supplementary information (Table S1). The “Baseline” model (“Baseline” in Figure 1) only considers the reaction of $\text{NO} + \text{OH}$ and the uptake of NO_2 on aerosol surfaces and subsequent transformation to HONO as the HONO sources. The low NO_x levels observed (around 13 p.p.t.v.) and the low uptake, however, prevent any significant HONO formation via R7, R8 and R8'.^{15, 40, 41} Therefore, the observed HONO levels of several p.p.t.v. are much larger than a photo-steady-state HONO level (below 0.01 p.p.t.v.) calculated by the “Baseline” model just considering R7, R8 and R8' alone with an upper limit uptake coefficient of NO_2 of 10^{-4} .¹⁵



The “Photolytic” model (Figure 1) is able to reproduce the observations when a typical mixing ratio of particulate nitrate of 280 p.p.t.v. (ca. $0.71 \mu\text{g m}^{-3}$) (Table S1), and a noontime photolysis rate constant of $1.1 \times 10^{-5} \text{ s}^{-1}$ for particulate nitrate to produce HONO is used.^{15, 39} At solar noon, the corresponding gaseous HNO_3 photolysis rate constant is $\sim 7.0 \times 10^{-7} \text{ s}^{-1}$,¹⁵ for Cape Verde and by normalising $j_{\text{pNitrate} \rightarrow \text{HONO}}$ to j_{HNO_3} (Eq. 5), the $j_{\text{pNitrate} \rightarrow \text{HONO}}^N$ determined may be compared to previous reported values. The “Photolytic” model, in comparison with the “Baseline” model, highlights the dominant role of particulate nitrate photolysis as an *in situ* HONO source (R3) in sustaining the photolytic loss of HONO in the MBL at CVAO, in agreement with the “NOMADSS scenario” (R3 and Eq. 2).

$$j_{pNitrate \rightarrow HONO}^N = j_{pNitrate \rightarrow HONO} \times \frac{7.0 \times 10^{-7} s^{-1}}{j_{HNO_3}} \quad (Eq. 5)$$

The normalized photolysis rate constant ($j_{pNitrate \rightarrow HONO}^N$) required to reproduce the HONO levels observed in CVAO was only around one sixth of the value used in the “NOMADSS scenario” (Table S1), however.¹⁵ The different $j_{pNitrate \rightarrow HONO}^N$ in the two studies may be rationalised from the different HONO and particulate nitrate budgets: The daily-average mixing ratio of particulate nitrate measured by a filter impactor method at CVAO varied from 236 p.p.t.v. to 941 p.p.t.v.⁴² The variability reflects different air masses reaching the observatory, e.g., from Europe, Africa, or North America on different days.^{4, 42} These values were 4 - 10 times higher than the particulate nitrate observation in the “NOMADSS scenario”.^{15, 42} However, the average mixing ratio of HONO of about 5 p.p.t.v. was only about half that observed in the “NOMADSS scenario”. The observation of a lower HONO/particulate nitrate ratio during the RHaMBLe project, compared to the “NOMADSS scenario”, indicates a lower scaling factor (\emptyset), considering a similar ratio of $j_{surface\ nitrate}$ to j_{HONO} (“Constant” in Eq. 6) for both RHaMBLe and NOMADSS.

$$\emptyset \approx \frac{[HONO]}{[pNitrate]} \times \frac{j_{HONO}}{j_{surface\ nitrate}} \approx \frac{[HONO]}{[pNitrate]} \times Constant \quad (Eq. 6)$$

A lower scaling factor (\emptyset) means a lower $j_{pNitrate \rightarrow HONO}^N$ for the RHaMBLe project compared to the “NOMADSS scenario” following Eq. 4 and Eq.5. Different aerosol properties in the two different environments were observed. For example, a high abundance of alkaline sea spray aerosol was generated at CVAO with a mean concentration of $11.1 \pm 5.5 \mu g m^{-3}$, alongside transported urban/dust aerosol.^{4, 42} As such, the particulate nitrate/HNO₃ ratio was mostly higher than 10:1 during the RHaMBLe project, whereas this ratio in aged marine air was 1:1 in the “NOMADSS scenario”.¹⁵ The high alkalinity of aerosols at CVAO, also implied by cation and anion balance analysis from filter aerosol samples,³⁰ might suppress both particulate nitrate photolysis and HONO release to some extent.³⁷ Even for different days during the RHaMBLe project, changes in the anion-to-

cation ratio of aerosol and the size distribution of aerosols suggest that air masses of different origins were encountered,³⁰ leading to variable chemical composition and physical properties of the aerosols at CVAO.^{4, 42, 43} As a result, the $j^N_{pNitrate \rightarrow HONO}$ values required to balance the HONO budget varied, as did the scaling factor, \emptyset , which ranged from 0.004 to 0.077 during the RHaMBLe project, as shown in Figure S2. The variable $j^N_{pNitrate \rightarrow HONO}$ found here and in previous studies suggests $j^N_{pNitrate \rightarrow HONO}$ should be analyzed case by case, either by a well-constrained HONO budget analysis as we have done here for CVAO, or by direct laboratory measurements as in the “NOMADSS scenario”.¹⁵ Future laboratory measurement of $j^N_{pNitrate \rightarrow HONO}$ are needed and should be conducted as a function of light absorbing organic components, water content, aerosol acidity, and anion/cation components etc., in order to fully characterize the “matrix effect” on particulate nitrate photolysis.^{15, 37}

NO_x calculation. Figure 2 shows the observed and modelled diel profiles of NO and NO₂. The NO₂ mixing ratio was observed to be stable throughout the day on some days, but peaked a few hours after solar noon on other days. On average, the daytime NO₂ concentration was 11.1 (± 1.7) p.p.t.v.. The NO mixing ratio was observed to peak around noontime, with a mean value of 2.2 (± 2.0) p.p.t.v. and a nighttime minima ca. 0 p.p.t.v.. The diel profiles of NO and NO₂ observed during RHaMBLe are representative of NO and NO₂ observations at CVAO since 2006.⁴ The total NO_x concentration of around 13 p.p.t.v. at noontime is lower than the year-round average (typical between 20 p.p.t.v. and 30 p.p.t.v.), but a low NO_x level is typical for May and June, owing to a large fraction of pure Atlantic air masses in this season.⁴ The “Baseline” model predicts a noontime maximum of NO, but the peak value is very low (0.14 p.p.t.v) relative to the observations. The “Baseline” model also predicts a noontime minima of NO₂ of only around 0.6 p.p.t.v., decreasing from the constrained mixing ratio of NO₂ of 10 p.p.t.v. at 8:15 (local time) which is just after sunrise (“Baseline” in Fig. 2). The “Photolytic” model reproduces diurnal profiles of both NO₂ and NO within measurement and model uncertainties, by the addition of HONO and

NO₂ formation from particulate nitrate photolysis, but was unable to reproduce the nighttime NO₂ observations (“Photolytic” in Figure 2) which may be attributed to transport which was not considered in the model.

The observed noontime maximum of NO is typical for pristine environments, and is governed by NO₂ photolysis, given the substantially higher than zero NO₂ levels (~ 11 pptv) observed during the daytime.⁹ As photolysis of NO₂ was considered in the models, both the “Baseline” model and the “Photolytic” model could capture the bell-shaped diurnal profile of NO during the daytime. However, only the “Photolytic” model was able to reproduce the absolute concentration of NO, since $j_{pNitrate}$ included in the “Photolytic” model effectively offset the fast oxidation of NO_x via reactions, such as, R1, R2 and R5, and reproduced the NO₂ observation.

The budget terms for NO_x in global models typically include physical processes (such as transport and deposition), emission, and chemical processing of reactive nitrogen species, such as NO_x, PAN, HNO₃ and CH₃ONO₂ (but usually not other RONO₂).^{1,9} These global models tend to reproduce NO₂ abundance in the nighttime if physical processes were considered, but would predict daytime minima of NO₂ abundance if no additional photochemical source of NO_x was considered, contrary to the observations.^{9,44} This suggests that transport, deposition and emission were mainly responsible for the nighttime NO₂ abundance, but were unable to account for both the abundance and diurnal profile of NO₂ during the daytime even with the chemical schemes in global model, e.g., the oxidation routes of NO_x mainly via R2 and R5, and photolytic losses of NO_x.^{4,9} The 0-D box model cannot reproduce nighttime NO₂ observations here because transport and emissions are not considered, and instead to represent the nighttime NO₂ levels, the model was constrained to measured values at 8.15 am. In the near-explicit MCM mechanism, the inclusion of comprehensive alkyl nitrate chemistry schemes and halogen chemistry schemes (R1 and R2), serves to enhance NO_x loss more so than models, e.g. the global model which typically do not consider these reactions.⁹ As shown in in the “Baseline” model in Figure 2, these losses lead to a fast decay of NO₂ after 8.15 am (when the model is constrained) as oxidants (OH, RO₂ and BrO

etc.) start to accumulate, and results in a minimum in NO_2 at noon which is at odds with the observations. The lack of a noontime minimum in the NO_2 observations (Figure 2b) indicates a missing NO_x source in the models.^{4,9} The transport of NO_x or NO_x reservoir species cannot fully account for the missing NO_x source during the daytime as CVAO is far away from any emission source of NO_x and its reservoirs, such as PAN, would mostly be consumed before reaching CVAO.⁴ Furthermore, NO_x reservoir species (e.g. PAN) have been observed to peak during the noontime, and thus would be expected to behave as noontime NO_x sinks, rather than noontime NO_x sources.^{4,6,13} The flat diurnal profile of total reactive nitrogen observed in the RHaMBLe project (not shown) suggests that the missing NO_x source was recycled from NO_x reservoir species, rather than rather than transported.⁴ With the production of HONO and NO_2 from particulate nitrate photolysis, the observation and model discrepancy can be reconciled, suggesting that this novel NO_x recycling route is a potential candidate for the missing NO_x source.

As stated in the “Model calculation” section, $j_{p\text{Nitrate}\rightarrow\text{NO}_2}$ was determined by balancing the NO_x budget, which is represented by Eq. 2'. A normalised $j_{p\text{Nitrate}\rightarrow\text{NO}_2}^N$ of $8 \times 10^{-7} \text{ s}^{-1}$ was employed in the box model in order to reproduce NO_x observations. The value of $j_{p\text{Nitrate}\rightarrow\text{NO}_2}^N$ was in fact small compared to the $j_{p\text{Nitrate}\rightarrow\text{HONO}}^N$ of $1.1 \times 10^{-5} \text{ s}^{-1}$. To compare, the HONO/ NO_2 production ratio from particulate nitrate photolysis was 2:1 in the “NOMADSS scenario”.¹⁵ The variation of the HONO/ NO_2 production ratio in the RHaMBLe project and the “NOMADSS scenario” must be due to the different physical-chemical properties of aerosol as it is stated above, but the higher-than-one ratio of HONO/ NO_2 production rate in both measurements confirm that HONO is an important intermediate to NO_x in particulate nitrate photolysis in pristine marine environments, and thus highlights the importance of HONO measurements for future NO_x budget analysis.

NO_x budget analysis. Figure 3 shows the diel profile of the rate of production and loss of NO_x . Particulate nitrate photolysis is the dominant NO_x source. The same conclusion was drawn during the NOMADSS study, highlighting the dominant role of particulate nitrate photolysis in sustaining NO_x levels in the pristine MBL.¹⁵ NO_x was mainly

lost by reactions with BrO, IO, OH and RO₂, leading to the formation of BrONO₂ (“Bromine Nitrate” in Figure 3), IONO₂ (“Iodine Nitrate”), HNO₃ (“Nitric acid”), and alkyl nitrates (“ANs”) respectively.^{12-14, 33} The competition between hydrolysis and photolysis determined the fate of BrONO₂ and IONO₂ with photolysis leading to the regeneration of NO₂ whilst hydrolysis on aerosols led to the formation of particulate nitrate (R1 and R1’).³⁴ Only hydrolysis of BrONO₂ and IONO₂ is considered as the net NO_x loss route in this study. BrO and IO were constrained in the model from DOAS observations, and the noontime maximum of BrO and IO mixing ratios were 3 p.p.t.v and 2 p.p.t.v., respectively.^{1, 31} HNO₃ was formed mainly via the gas phase reaction of OH with NO₂ (R5). The dominate sink of HNO₃ at CVAO was the uptake by alkaline sea spray aerosol, as indicated from the high particulate nitrate/HNO₃ ratio. Alkyl nitrates were formed via the side reactions between RO₂ radicals and NO (R6’). The fate of organic nitrates was partly hydrolytic loss on aerosols in the MBL as the latest studies have suggested.¹²⁻¹⁴ These NO_x sinks were calculated either using observational terms (such as BrO and IO) or by modelled terms which was in agreement with observations (such as OH).²³

Compared to the “NOMADSS scenario”, the high levels of BrO, IO and aerosol loading at CVAO favoured high oxidative losses of NO₂ via BrONO₂ and IONO₂ formation and hydrolysis (Table S1). Both the total production and destruction rates of NO_x in the noontime reached nearly 30 p.p.t.v. h⁻¹, which suggests a NO_x lifetime of around half an hour and photolysis lifetime for particulate nitrate of around 9 h. The fast cycling rate between particulate nitrate and NO_x suggests that particulate nitrate is a NO_x reservoir rather than a permanent sink of NO_x. Particulate nitrate can transport NO_x over long distances similar to other NO_x reservoir species, and by this mechanism can greatly influence NO_x levels especially during the daytime as shown here, and thus influences the oxidation capacity downwind of emission sources.

Atmospheric implications. Traditionally, NO_x emission controls have been essential in controlling the O₃ burden in the free troposphere and in the remote atmospheric boundary layer. The ozone production efficiency (OPE, i.e. ozone production per unit NO_x emission or NO_x degradation in Eq. 7) was defined to evaluate the O₃

formation burden, based on known NO_x emission inventories.⁴⁶ With this novel NO_x recycling route, the effective lifetime of NO_x is actually much longer than previously thought, and the definition of OPE, therefore, should be updated to account for this. A correction factor (OPE C factor in Eq. 8) describes how many times NO_x is recycled via particulate nitrate photolysis before the total reactive nitrogen being removed via deposition permanently from the atmosphere:

$$OPE = \frac{\text{ozone production rate}}{NO_x \text{ oxidation rate}} = \frac{k_{NO+HO_2}[NO][HO_2] + \sum_i k_{NO+R_iO_2}[NO][HO_2]}{NO_x \text{ oxidation rate}} \quad (Eq. 7)$$

$$OPE \text{ C factor (\%)} = \frac{[pNitrate] \times j_{pNitrate}}{\text{deposition rate} \times [NO_y]} \times 100 \quad (Eq. 8)$$

where k_{NO+HO_2} and $k_{NO+R_iO_2}$ are the rate constants of reactions of NO with HO₂ and various RO₂ radicals, respectively. The OPE C factor reflects the competition between NO_x recycling and depositional losses. It would thus change with both photolysis rate and deposition rate in different environments. In the MBL at CVAO, the OPE C factor reaches nearly 500% in the noontime if a deposition velocity of 2 cm s⁻¹ is assumed for all reactive nitrogen species (Figure 4).³⁴ The high partitioning ratio of total nitrate (sum of gas phase HNO₃ and particulate nitrate) to particulate nitrate here contributes greatly to the cycling rate of total nitrate, as the photolysis rate constant of particulate nitrate is orders of magnitude faster than the photolysis rate of gas phase HNO₃.

The perturbation to O₃ chemistry by this recycling of NO_x can be considered by considering the perturbation this recycling makes to the O₃ production rate. The recycling of NO_x from particulate nitrate photolysis is the dominant NO_x source; while other well-known NO_x reservoirs, such as PAN and HO₂NO₂, which were present at the low p.p.t.v. level, only play a minor and possibly negative role in sustaining the NO_x level in the MBL in the daytime at a temperature of 23-24 °C.⁴ Therefore, this recycling of NO_x from particulate nitrate dominates O₃ formation in the pristine marine environment. Figure 4 show that in this study, the O₃ production term reached ca. 200 p.p.t.v. h⁻¹ in the noontime when this recycling term is considered, compared to

a O_3 production rate of Ca. 2 p.p.t.v.h^{-1} calculated in the baseline model. This O_3 formation rate needs to be considered to fully and correctly determine the net O_3 depletion rate in the MBL.¹

In summary, our results suggest a dominant role of particulate nitrate photolysis in the NO_x budget in the pristine MBL. Considering the role of NO_x on O_3 formation, O_3 calculations by global models should in the future consider this NO_x recycling mechanism. In addition, our model study highlights the importance of HONO measurements as a NO_x budget constraint in the pristine MBL, and there is an urgent need for the determination of the photolysis rate constant of particulate nitrate in various environments or under controlled laboratory conditions.

ACKNOWLEDGEMENTS

The authors would like to thank the open source data archive, participating scientists, and supporting staff in the RHaMBLe project. We would also like to thank Lucy Carpenter, James Lee and Chris Reed (University of York) for useful discussions. We are also grateful to the UK Natural Environment Research Council for funding (grant number NE/K012029/1).

FIGURES

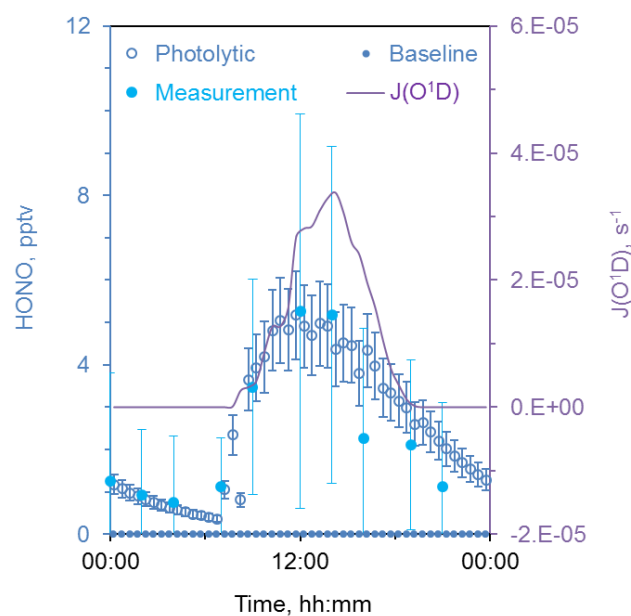


Figure 1. Diel profile of calculated HONO by the “Baseline” and the “Photolytic” 0-D box model, measured $J(O^1D)$ and measured HONO concentration during the RHaMBLe project from May 18th – June 15th 2007 at CVAO. The HONO error bars indicate the standard deviation of measured or modelled HONO during the RHaMBLe project. The daytime HONO peak of around 0.004 p.p.t.v. calculated by the “Baseline” model is too small to be seen on this figure. The error bar ($\pm 35\%$) for the baseline model result is too small to be seen on this figure.

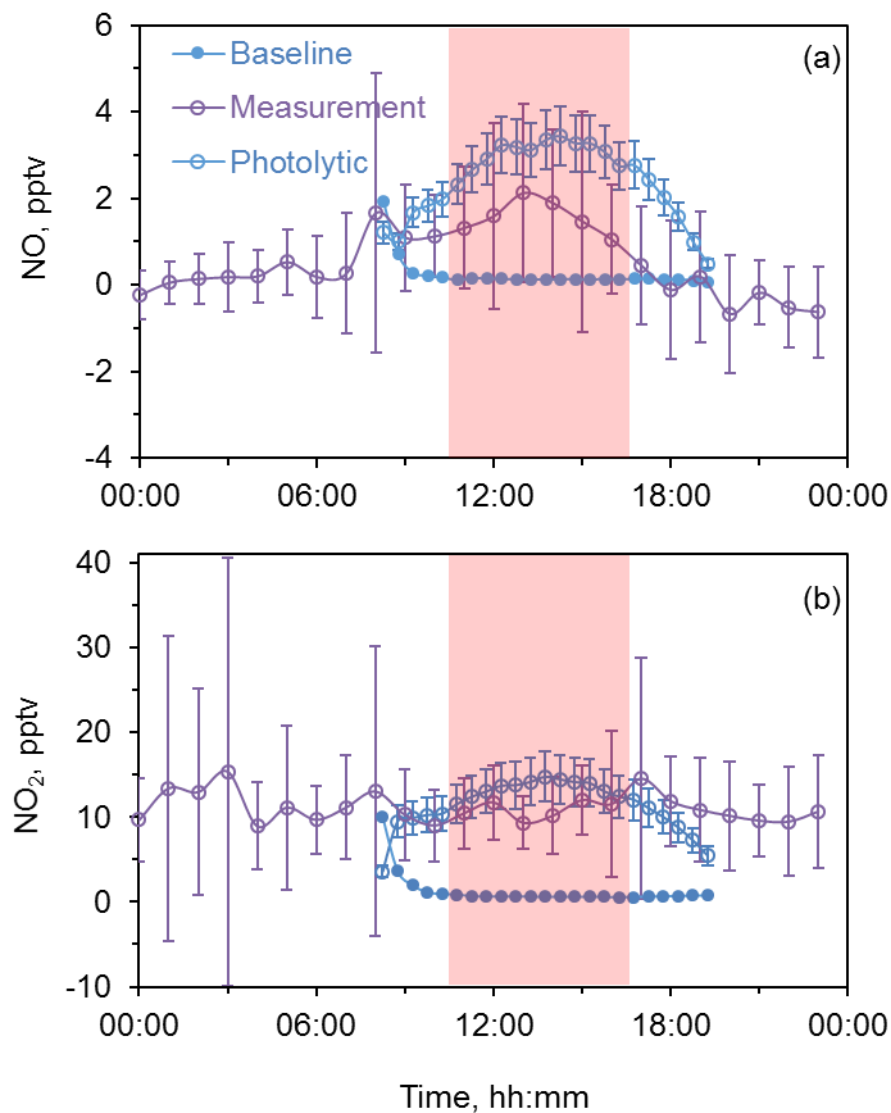


Figure 2. Diel profiles of calculated NO (a) and NO₂ (b) abundance using the “Baseline” and the “Photolytic” model, and the corresponding measured NO and NO₂ abundances during the RHaMBLe project at CVAO. See text for details of the model scenarios. The noontime peak of NO and noontime minimum of NO₂ calculated by “Baseline” model is too small to be observed on the current graph scale. The red shading represents the defined “daytime” period for the model which is from 10:00 to 16:00 (Local time, being from 2 hours after sunrise to 2 hours before sunset).

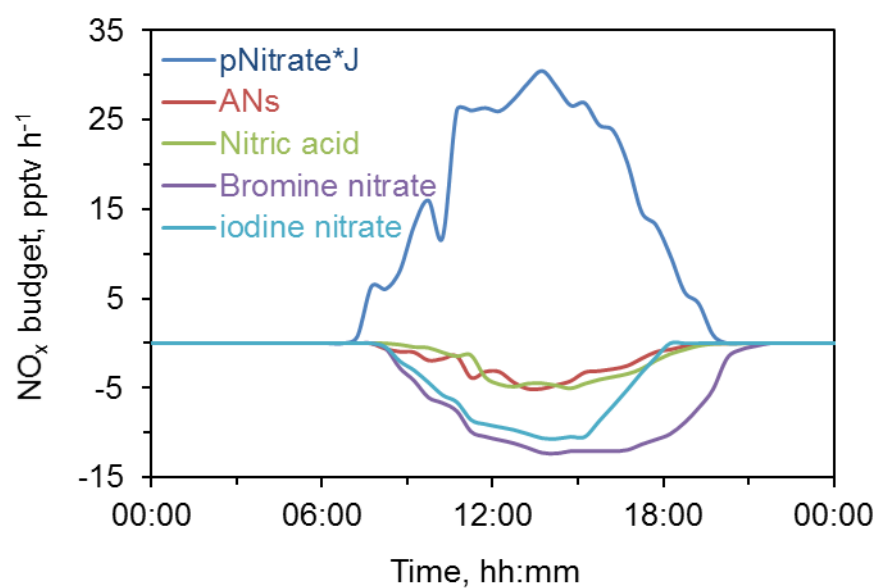


Figure 3. Diel profiles of the rate of NO_x production and loss calculated by the 0-D box model based on averages of measurements in the RHaMBLe project. “pNitrate*J” represents the particulate nitrate photolysis rate at Cape Verde, defined by equation 3 and 3’. “ANs”, “Nitric acid”, “Bromine nitrate” and “Iodine nitrate” represent the main NO_x sinks via formation and hydrolysis of alkyl nitrates, nitric acid, bromine nitrate and iodine nitrate, respectively.

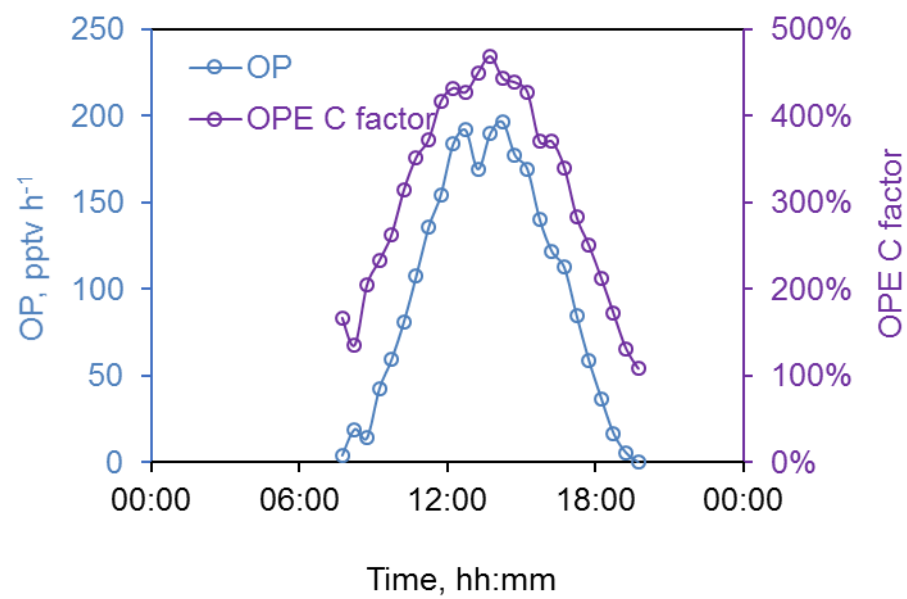


Figure 4. Diurnals of ozone formation rate (OP) calculated using Eq. 7 and the ozone production efficiency correction factor (OPE C factor, defined by Eq. 8), averaged during the RHaMBLe project.

SUPPLEMENTARY INFORMATION

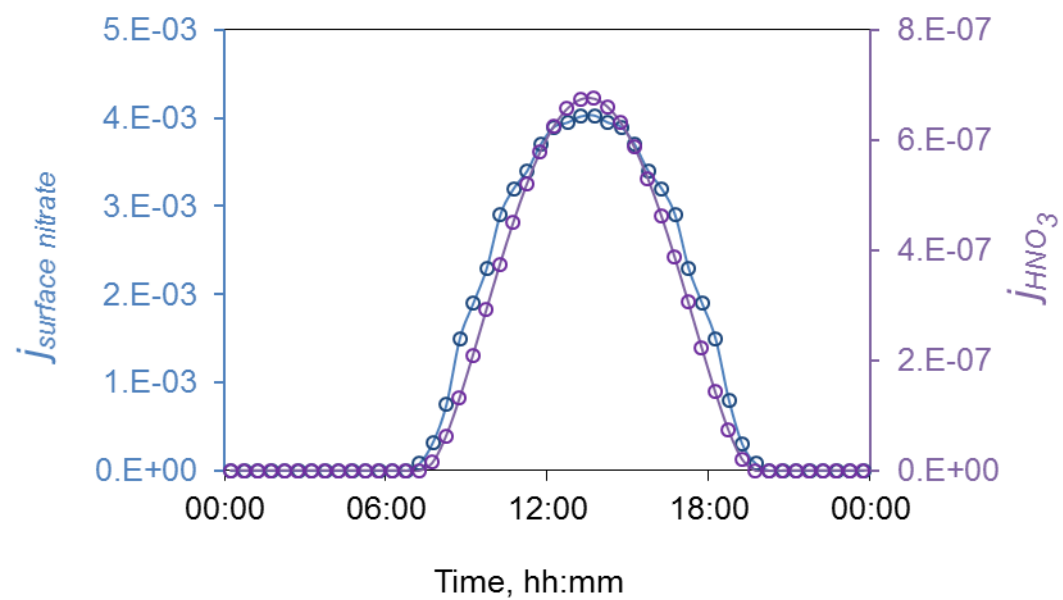


Figure S1. Diel profiles of the photolysis rate constants of gas-phase HNO_3 (j_{HNO_3}) and surface HNO_3 ($j_{\text{surface nitrate}}$) based on the cross section and quantum yield of surface nitrate on silicon between 290-365 nm.^{35, 36}

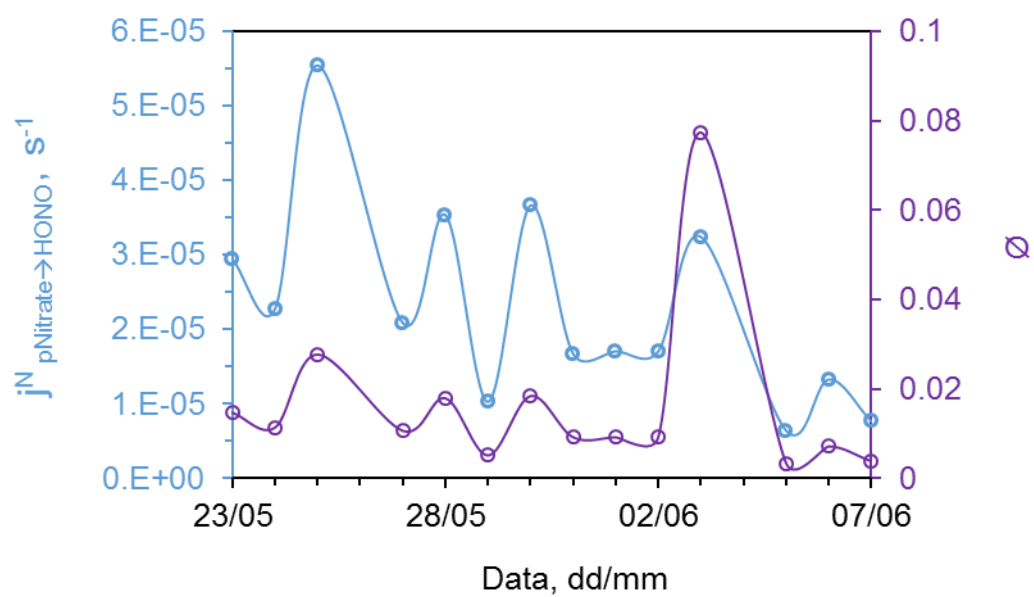


Figure S2. The variability of normalized $j_{pNitrate \rightarrow HONO}^N$ and the ratio of $j_{pNitrate \rightarrow HONO}$ to $j_{surface\ nitrate}$ (the scaling factor \emptyset in Eq. 4) on different days during the 2007 RHaMBLe project. The reasons for the variability are explained in the main paper text (section “HONO calculation”).

Table S1. Comparison of the conditions for two background marine boundary layer, namely Cape Verde in the RHaMBLe study (used in this study) and the North Atlantic Ocean in the NOMADSS study.¹⁵ The RHaMBLe measurements were from May 18th – June 15th 2007.

	[NO _x] /pptv	[HONO] /pptv	[Particulate Nitrate] /pptv	$j^N_{pNitrate \rightarrow HONO}$ ^c /s ⁻¹	Air mass origin
RHaMBLe ^a	~ 13	~ 5	236 - 941	0.11×10 ⁻⁴	Atlantic air/transport
NOMADSS ^b	~ 30	8 - 12	27 - 80	0.66×10 ⁻⁴	Pure Atlantic air

Note:

^a For *RHaMBLe*, [NO_x] represents an daytime average between 10:00 and 16:00, where [HONO] represents the noontime maximum of HONO measurements.

^b Values in the “NOMADSS scenario” were from two-day noontime measurements in the NOMADSS project.¹⁵

^c $j^N_{pNitrate \rightarrow HONO}$ is the normalized noontime value which was scaled to the typical tropical summer conditions on the ground (solar elevation angle $\theta = 0^\circ$), corresponding to a gaseous HNO₃ photolysis rate constant of $\sim 7.0 \times 10^{-7} \text{ s}^{-1}$.¹⁵ Therefore, $j^N_{pNitrate \rightarrow HONO}$ could be directly compared on different days during the RHaMBLe project, and with literature reported values.

REFERENCES

1. Read, K. A.; Mahajan, A. S.; Carpenter, L. J.; Evans, M. J.; Faria, B. V. E.; Heard, D. E.; Hopkins, J. R.; Lee, J. D.; Moller, S. J.; Lewis, A. C.; Mendes, L.; McQuaid, J. B.; Oetjen, H.; Saiz-Lopez, A.; Pilling, M. J.; Plane, J. M. C., Extensive halogen-mediated ozone destruction over the tropical Atlantic Ocean. *Nature* **2008**, *453*, (7199), 1232-1235.
2. Parrish, D. D.; Lamarque, J. F.; Naik, V.; Horowitz, L.; Shindell, D. T.; Staehelin, J.; Derwent, R.; Cooper, O. R.; Tanimoto, H.; Volz-Thomas, A.; Gilge, S.; Scheel, H. E.; Steinbacher, M.; Frohlich, M., Long-term changes in lower tropospheric baseline ozone concentrations: Comparing chemistry-climate models and observations at northern midlatitudes. *Journal of Geophysical Research-Atmospheres* **2014**, *119*, (9), 5719-5736.
3. Martin, M. V.; Heald, C. L.; Arnold, S. R., Coupling dry deposition to vegetation phenology in the Community Earth System Model: Implications for the simulation of surface O₃. *Geophysical Research Letters* **2014**, *41*, (8), 2988-2996.
4. Lee, J. D.; Moller, S. J.; Read, K. A.; Lewis, A. C.; Mendes, L.; Carpenter, L. J., Year-round measurements of nitrogen oxides and ozone in the tropical North Atlantic marine boundary layer. *Journal of Geophysical Research-Atmospheres* **2009**, *114*, D21302.
5. Seltzer, K. M.; Vizuete, W.; Henderson, B. H., Evaluation of updated nitric acid chemistry on ozone precursors and radiative effects. *Atmos Chem Phys* **2015**, *15*, (10), 5973-5986.
6. Jacobi, H. W.; Weller, R.; Bluszczyk, T.; Schrems, O., Latitudinal distribution of peroxyacetyl nitrate (PAN) over the Atlantic Ocean. *Journal of Geophysical Research-Atmospheres* **1999**, *104*, (D21), 26901-26912.
7. Singh, H. B.; Salas, L.; Herlth, D.; Kolyer, R.; Czech, E.; Avery, M.; Crawford, J. H.; Pierce, R. B.; Sachse, G. W.; Blake, D. R.; Cohen, R. C.; Bertram, T. H.; Perring, A.; Wooldridge, P. J.; Dibb, J.; Huey, G.; Hudman, R. C.; Turquety, S.; Emmons, L. K.; Flocke, F.; Tang, Y.; Carmichael, G. R.; Horowitz, L. W., Reactive nitrogen distribution and partitioning in the North American troposphere and lowermost stratosphere. *Journal of Geophysical Research-Atmospheres* **2007**, *112*, (D12), D12S04.
8. Napelenok, S. L.; Pinder, R. W.; Gilliland, A. B.; Martin, R. V., A method for evaluating spatially-resolved NO_x emissions using Kalman filter inversion, direct sensitivities, and space-based NO₂ observations. *Atmos Chem Phys* **2008**, *8*, (18), 5603-5614.
9. Pike, R. C.; Lee, J. D.; Young, P. J.; Carver, G. D.; Yang, X.; Warwick, N.; Moller, S.; Misztal, P.; Langford, B.; Stewart, D.; Reeves, C. E.; Hewitt, C. N.; Pyle, J. A., NO_x and O₃ above a tropical rainforest: an analysis with a global and box model. *Atmos Chem Phys* **2010**, *10*, (21), 10607-10620.
10. Heald, C. L.; Collett, J. L.; Lee, T.; Benedict, K. B.; Schwandner, F. M.; Li, Y.; Clarisse, L.; Hurtmans, D. R.; Van Damme, M.; Clerbaux, C.; Coheur, P. F.; Philip, S.; Martin, R. V.; Pye, H. O. T., Atmospheric ammonia and particulate inorganic nitrogen over the United States. *Atmos Chem Phys* **2012**, *12*, (21), 10295-10312.
11. Henderson, B. H.; Pinder, R. W.; Crooks, J.; Cohen, R. C.; Hutzell, W. T.; Sarwar, G.; Goliff, W. S.; Stockwell, W. R.; Fahr, A.; Mathur, R.; Carlton, A. G.; Vizuete, W., Evaluation of simulated photochemical partitioning of oxidized nitrogen in the upper troposphere. *Atmos Chem Phys* **2011**, *11*, (1), 275-291.
12. Romer, P. S.; Duffey, K. C.; Wooldridge, P. J.; Allen, H. M.; Ayres, B. R.; Brown, S. S.; Brune, W. H.; Crouse, J. D.; de Gouw, J.; Draper, D. C.; Feiner, P. A.; Fry, J. L.; Goldstein, A. H.; Koss, A.; Misztal, P. K.; Nguyen, T. B.; Olson, K.; Teng, A. P.; Wennberg, P. O.; Wild, R. J.; Zhang, L.; Cohen, R. C., The lifetime of nitrogen oxides in an isoprene-dominated forest. *Atmos. Chem. Phys.* **2016**, *16*, (12), 7623-7637.
13. Perring, A. E.; Pusede, S. E.; Cohen, R. C., An Observational Perspective on the Atmospheric Impacts of Alkyl and Multifunctional Nitrates on Ozone and Secondary Organic Aerosol. *Chemical Reviews* **2013**, *113*, (8), 5848-5870.
14. Browne, E. C.; Min, K. E.; Wooldridge, P. J.; Apel, E.; Blake, D. R.; Brune, W. H.; Cantrell, C. A.; Cubison, M. J.; Diskin, G. S.; Jimenez, J. L.; Weinheimer, A. J.; Wennberg, P. O.; Wisthaler, A.; Cohen, R. C., Observations of total RONO₂ over the boreal forest: NO_x sinks and HNO₃ sources. *Atmos Chem Phys* **2013**, *13*, (9), 4543-4562.
15. Ye, C. X.; Zhou, X. L.; Pu, D.; Stutz, J.; Festa, J.; Spolaor, M.; Tsai, C.; Cantrell, C.; Mauldin, R. L.; Campos, T.; Weinheimer, A.; Hornbrook, R. S.; Apel, E. C.; Guenther, A.; Kaser, L.; Yuan, B.; Karl, T.; Haggerty, J.; Hall, S.; Ullmann, K.; Smith, J. N.; Ortega, J.; Knote, C., Rapid cycling of reactive nitrogen in the marine boundary layer. *Nature* **2016**, *532*, (7600), 489-491.

16. Saunders, S. M.; Jenkin, M. E.; Derwent, R. G.; Pilling, M. J., Protocol for the development of the Master Chemical Mechanism, MCM v3 (Part A): tropospheric degradation of non-aromatic volatile organic compounds. *Atmos Chem Phys* **2003**, *3*, 161-180.
17. Reed, C.; Evans, M. J.; Di Carlo, P.; Lee, J. D.; Carpenter, L. J., Interferences in photolytic NO₂ measurements: explanation for an apparent missing oxidant? *Atmos Chem Phys* **2016**, *16*, (7), 4707-4724.
18. Bloss, W. J.; Camredon, M.; Lee, J. D.; Heard, D. E.; Plane, J. M. C.; Saiz-Lopez, A.; Bauguitte, S. J. B.; Salmon, R. A.; Jones, A. E., Coupling of HO_x, NO_x and halogen chemistry in the antarctic boundary layer. *Atmos Chem Phys* **2010**, *10*, (21), 10187-10209.
19. Baergen, A. M.; Donaldson, D. J., Photochemical Renoxification of Nitric Acid on Real Urban Grime. *Environ Sci Technol* **2013**, *47*, (2), 815-820.
20. Baergen, A. M.; Donaldson, D. J., Formation of reactive nitrogen oxides from urban grime photochemistry. *Atmos Chem Phys* **2016**, *16*, (10), 6355-6363.
21. Carpenter, L. J.; Fleming, Z. L.; Read, K. A.; Lee, J. D.; Moller, S. J.; Hopkins, J. R.; Purvis, R. M.; Lewis, A. C.; Muller, K.; Heinold, B.; Herrmann, H.; Fomba, K. W.; van Pinxteren, D.; Muller, C.; Tegen, I.; Wiedensohler, A.; Muller, T.; Niedermeier, N.; Achterberg, E. P.; Patey, M. D.; Kozlova, E. A.; Heimann, M.; Heard, D. E.; Plane, J. M. C.; Mahajan, A.; Oetjen, H.; Ingham, T.; Stone, D.; Whalley, L. K.; Evans, M. J.; Pilling, M. J.; Leigh, R. J.; Monks, P. S.; Karunaharan, A.; Vaughan, S.; Arnold, S. R.; Tschritter, J.; Pohler, D.; Friess, U.; Holla, R.; Mendes, L. M.; Lopez, H.; Faria, B.; Manning, A. J.; Wallace, D. W. R., Seasonal characteristics of tropical marine boundary layer air measured at the Cape Verde Atmospheric Observatory. *Journal of Atmospheric Chemistry* **2010**, *67*, (2-3), 87-140.
22. Lee, J. D.; McFiggans, G.; Allan, J. D.; Baker, A. R.; Ball, S. M.; Benton, A. K.; Carpenter, L. J.; Commane, R.; Finley, B. D.; Evans, M.; Fuentes, E.; Furneaux, K.; Goddard, A.; Good, N.; Hamilton, J. F.; Heard, D. E.; Herrmann, H.; Hollingsworth, A.; Hopkins, J. R.; Ingham, T.; Irwin, M.; Jones, C. E.; Jones, R. L.; Keene, W. C.; Lawler, M. J.; Lehmann, S.; Lewis, A. C.; Long, M. S.; Mahajan, A.; Methven, J.; Moller, S. J.; Muller, K.; Muller, T.; Niedermeier, N.; O'Doherty, S.; Oetjen, H.; Plane, J. M. C.; Pszenny, A. A. P.; Read, K. A.; Saiz-Lopez, A.; Saltzman, E. S.; Sander, R.; von Glasow, R.; Whalley, L.; Wiedensohler, A.; Young, D., Reactive Halogens in the Marine Boundary Layer (RHaMBLe): the tropical North Atlantic experiments. *Atmos Chem Phys* **2010**, *10*, (3), 1031-1055.
23. Whalley, L. K.; Furneaux, K. L.; Goddard, A.; Lee, J. D.; Mahajan, A.; Oetjen, H.; Read, K. A.; Kaaden, N.; Carpenter, L. J.; Lewis, A. C.; Plane, J. M. C.; Saltzman, E. S.; Wiedensohler, A.; Heard, D. E., The chemistry of OH and HO₂ radicals in the boundary layer over the tropical Atlantic Ocean. *Atmos Chem Phys* **2010**, *10*, (4), 1555-1576.
24. Read, K. A.; Lee, J. D.; Lewis, A. C.; Moller, S. J.; Mendes, L.; Carpenter, L. J., Intra-annual cycles of NMVOC in the tropical marine boundary layer and their use for interpreting seasonal variability in CO. *Journal of Geophysical Research-Atmospheres* **2009**, *114*, D21303.
25. Keene, W. C.; Stutz, J.; Pszenny, A. A. P.; Maben, J. R.; Fischer, E. V.; Smith, A. M.; von Glasow, R.; Pechtl, S.; Sive, B. C.; Varner, R. K., Inorganic chlorine and bromine in coastal New England air during summer. *Journal of Geophysical Research-Atmospheres* **2007**, *112*, (D10), D10S12.
26. Birmili, W.; Yuskiewicz, B.; Wiedensohler, A.; Stratmann, F.; Choularton, T. W.; Bower, K. N., Climate-relevant modification of the aerosol size distribution by processes associated with orographic clouds. *Atmospheric Research* **1999**, *50*, (3-4), 241-263.
27. Kozlova, E. A.; Manning, A. C., Methodology and calibration for continuous measurements of biogeochemical trace gas and O₂ concentrations from a 300-m tall tower in central Siberia. *Atmospheric Measurement Techniques* **2009**, *2*, (1), 205-220.
28. Simmonds, P. G.; Derwent, R. G.; Manning, A. J.; Fraser, P. J.; Krummel, P. B.; O'Doherty, S.; Prinn, R. G.; Cunnold, D. M.; Miller, B. R.; Wang, H. J.; Ryall, D. B.; Porter, L. W.; Weiss, R. F.; Salameh, P. K., AGAGE observations of methyl bromide and methyl chloride at Mace Head, Ireland, and Cape Grim, Tasmania, 1998-2001. *Journal of Atmospheric Chemistry* **2004**, *47*, (3), 243-269.
29. Hough, A. M., The calculation of photolysis rates for use in global tropospheric modelling studies. *AERE rep.* **1988**, *Her Majesty's Stn. Off., Norwich*.
30. Muller, K.; Lehmann, S.; van Pinxteren, D.; Gnauk, T.; Niedermeier, N.; Wiedensohler, A.; Herrmann, H., Particle characterization at the Cape Verde atmospheric observatory during the 2007 RHaMBLe intensive. *Atmos Chem Phys* **2010**, *10*, (6), 2709-2721.

31. Mahajan, A. S.; Plane, J. M. C.; Oetjen, H.; Mendes, L.; Saunders, R. W.; Saiz-Lopez, A.; Jones, C. E.; Carpenter, L. J.; McFiggans, G. B., Measurement and modelling of tropospheric reactive halogen species over the tropical Atlantic Ocean. *Atmos Chem Phys* **2010**, *10*, (10), 4611-4624.
32. Vaughan, S.; Ingham, T.; Whalley, L. K.; Stone, D.; Evans, M. J.; Read, K. A.; Lee, J. D.; Moller, S. J.; Carpenter, L. J.; Lewis, A. C.; Fleming, Z. L.; Heard, D. E., Seasonal observations of OH and HO₂ in the remote tropical marine boundary layer. *Atmos Chem Phys* **2012**, *12*, (4), 2149-2172.
33. Savarino, J.; Morin, S.; Erbland, J.; Grannec, F.; Patey, M. D.; Vicars, W.; Alexander, B.; Achterberg, E. P., Isotopic composition of atmospheric nitrate in a tropical marine boundary layer. *Proceedings of the National Academy of Sciences of the United States of America* **2013**, *110*, (44), 17668-17673.
34. Burkholder, J. B.; Sander, S. P.; Abbatt, J. P. D.; Barker, J. R.; Huie, R. E.; Kolb, C. E.; Kurylo, M. J.; Orkin, V. L.; Wilmouth, D. M.; Wine, P. H., Chemical Kinetics and Photochemical Data for use in Atmospheric Studies - Evaluation Number 18. *JPL Publication 15-10, Jet Propulsion Laboratory, Pasadena* **2015**, <http://jpldataeval.jpl.nasa.gov>.
35. Zhu, C. Z.; Xiang, B.; Zhu, L.; Cole, R., Determination of absorption cross sections of surface-adsorbed HNO₃ in the 290-330 nm region by Brewster angle cavity ring-down spectroscopy. *Chemical Physics Letters* **2008**, *458*, (4-6), 373-377.
36. Du, J.; Zhu, L., Quantification of the absorption cross sections of surface-adsorbed nitric acid in the 335-365 nm region by Brewster angle cavity ring-down spectroscopy. *Chemical Physics Letters* **2011**, *511*, (4-6), 213-218.
37. Ye, C. X.; Gao, H. L.; Zhang, N.; Zhou, X. L., Photolysis of Nitric Acid and Nitrate on Natural and Artificial Surfaces. *Environ Sci Technol* **2016**, *50*, (7), 3530-3536.
38. Beygi, Z. H.; Fischer, H.; Harder, H. D.; Martinez, M.; Sander, R.; Williams, J.; Brookes, D. M.; Monks, P. S.; Lelieveld, J., Oxidation photochemistry in the Southern Atlantic boundary layer: unexpected deviations of photochemical steady state. *Atmos Chem Phys* **2011**, *11*, (16), 8497-8513.
39. Sander, R.; Pszenny, A. A. P.; Keene, W. C.; Crete, E.; Deegan, B.; Long, M. S.; Maben, J. R.; Young, A. H., Gas phase acid, ammonia and aerosol ionic and trace element concentrations at Cape Verde during the Reactive Halogens in the Marine Boundary Layer (RHAMBLe) 2007 intensive sampling period. *Earth System Science Data* **2013**, *5*, (2), 385-392.
40. Ye, C. X.; Zhou, X. L.; Pu, D.; Stutz, J.; Festa, J.; Spolaor, M.; Cantrell, C.; Mauldin, R. L.; Weinheimer, A.; Haggerty, J., Comment on "Missing gas-phase source of HONO inferred from Zeppelin measurements in the troposphere". *Science* **2015**, *348*, (6241), 1326.
41. Li, X.; Rohrer, F.; Hofzumahaus, A.; Brauers, T.; Haseler, R.; Bohn, B.; Broch, S.; Fuchs, H.; Gomm, S.; Holland, F.; Jager, J.; Kaiser, J.; Keutsch, F. N.; Lohse, I.; Lu, K. D.; Tillmann, R.; Wegener, R.; Wolfe, G. M.; Mentel, T. F.; Kiendler-Scharr, A.; Wahner, A., Missing Gas-Phase Source of HONO Inferred from Zeppelin Measurements in the Troposphere. *Science* **2014**, *344*, (6181), 292-296.
42. Fomba, K. W.; Muller, K.; van Pinxteren, D.; Poulain, L.; van Pinxteren, M.; Herrmann, H., Long-term chemical characterization of tropical and marine aerosols at the Cape Verde Atmospheric Observatory (CVAO) from 2007 to 2011. *Atmos Chem Phys* **2014**, *14*, (17), 8883-8904.
43. Allan, J. D.; Topping, D. O.; Good, N.; Irwin, M.; Flynn, M.; Williams, P. I.; Coe, H.; Baker, A. R.; Martino, M.; Niedermeier, N.; Wiedensohler, A.; Lehmann, S.; Muller, K.; Herrmann, H.; McFiggans, G., Composition and properties of atmospheric particles in the eastern Atlantic and impacts on gas phase uptake rates. *Atmos Chem Phys* **2009**, *9*, (23), 9299-9314.
44. Bauguitte, S. J. B.; Bloss, W. J.; Evans, M. J.; Salmon, R. A.; Anderson, P. S.; Jones, A. E.; Lee, J. D.; Saiz-Lopez, A.; Roscoe, H. K.; Wolff, E. W.; Plane, J. M. C., Summertime NO_x measurements during the CHABLIS campaign: can source and sink estimates unravel observed diurnal cycles? *Atmos Chem Phys* **2012**, *12*, (2), 989-1002.